ChemComm

COMMUNICATION

View Article Online
View Journal | View Issue

Published on 25 February 2016. Downloaded by Iowa State University on 19/09/2016 03:29:56.

Cite this: *Chem. Commun.*, 2016, 52, 4239

Received 18th November 2015,
Accepted 15th February 2016

DOI: 10.1039/c5cc09434h

www.rsc.org/chemcomm

Elucidation of the surface characteristics and electrochemistry of high-performance $LiNiO_2$†

Jing Xu,[a] Feng Lin,[a] Dennis Nordlund,[b] Ethan J. Crumlin,[c] Feng Wang,[d] Jianming Bai,[e] Marca M. Doeff[a] and Wei Tong*[a]

Phase pure $LiNiO_2$ was prepared using a solid-state method and the optimal synthesis conditions led to a remarkably high capacity of 200 mA h g^{-1} with excellent retention. The combination of bulk and surface characterization elucidated an essential role of the excess Li in phase formation during synthesis and the subsequent electrochemical performance.

At present, Li-ion batteries are considered to be the most promising energy storage devices for electric vehicles (EVs) and plug-in hybrid electric vehicles (HEVs). However, the ultimate goals of high performance and low cost ($ per W h) need to be achieved in order to replace fuel by electrical power, and realize mass adoption of EVs and HEVs. $LiNiO_2$ attracted immediate attention in the initial search for alternatives to $LiCoO_2$ because of the isostructural characteristics and lower cost.[1] Moreover, the electronic configuration of Ni^{3+} ($3d^7$) in $LiNiO_2$ allows the removal of electrons only from the e_g band, so that loss of oxygen occurs at a lower Li content (x in Li_xMO_2, where M = Co or Ni), *i.e.*, at a higher charge state compared to $LiCoO_2$, which translates into higher practical capacity.[2] However, because of the higher Ni content, a severe capacity fading may occur upon cycling, due to the impacts of both structural transformation and surface instability.[3–6] A combination of different transition metals (*e.g.*, $LiNi_xMn_yCo_zO_2$ or NMCs) further increases the complexity of the problem since phase separation and side reactions with the electrolyte have been reported for different compositions.[7,8] Therefore, the elucidation of the structural characteristics and their relationship with the electrochemical behavior for pure $LiNiO_2$ not only provides insights into the synthesis of better performing $LiNiO_2$ compounds but also complements the mechanistic understanding of more complex R-3m layered compounds, such as nickel-rich NMC materials, by isolating the synergistic effects from different transition metals.

The synthesis of stoichiometric $LiNiO_2$ is challenging due to its tendency for lithium loss and migration of Ni to the lithium layers to form off-stoichiometric $Li_{1-x}Ni_{1+x}O_2$. The presence of excess Ni ions on the Li sites blocks the Li diffusion pathways and imposes a detrimental effect on the electrochemical performance.[9–11] Various conditions that are related to the synthetic routes have been explored and several key variables have been identified. For example, Ohzuku *et al.* investigated the effects of Li, Ni precursors, and annealing atmospheres on the synthesis of $LiNiO_2$ *via* solid state reactions and observed a pronounced effect of the O_2 atmosphere on the stoichiometry and cation arrangement.[12] Reacting $LiNO_3$ with $Ni(OH)_2$ or $NiCO_3$ at 750 °C under an O_2 atmosphere produced a product with an initial charge capacity of 180 mA h g^{-1} and a reversible discharge capacity of above 150 mA h g^{-1} in the voltage range of 2.5–4.2 V (0.17 mA cm^{-2}). Lu *et al.* further pointed out that a high O_2 partial pressure was necessary to overcome the diffusion barrier existing in the precursor powder.[13] When annealed at a high O_2 flow rate (800 mL min^{-1}), the $LiNiO_2$ product delivered a discharge capacity of >160 mA h g^{-1} with 150 mA h g^{-1} remained after 30 cycles (3.0–4.3 V, 0.4 mA cm^{-2}).[14] In addition, the Li content in the precursor also played a key role in the stoichiometry of the final product. Arai *et al.* reported the synthesis of a highly stoichiometric $LiNiO_2$ obtained by mixing an aqueous solution of $LiOH{\cdot}H_2O$ and $Ni(NO_3)_2{\cdot}6H_2O$ with a molar ratio of 4 : 1 and washing away the large amount of excess Li after calcination. This material delivered a reversible capacity of about 200 mA h g^{-1} during 10 cycles (3.0–4.5 V, 0.5 mA cm^{-2}).[15] These results suggest that the design of $LiNiO_2$ cathodes could benefit from a systematic study of the relationship between synthesis parameters, structural and chemical characteristics, and electrochemical behaviour.

[a] *Energy Storage and Distributed Resources Division, Lawrence Berkeley National Laboratory, Berkeley, CA 94720, USA. E-mail: weitong@lbl.gov*
[b] *Stanford Synchrotron Radiation Lightsource, SLAC National Accelerator Laboratory, Menlo Park, CA 94025, USA*
[c] *Advanced Light Source, Lawrence Berkeley National Laboratory, Berkeley, California 94720, USA*
[d] *Department of Sustainable Energy Technologies, Brookhaven National Laboratory, Upton, New York 11973, USA*
[e] *National Synchrotron Light Source II, Brookhaven National Laboratory, Upton, NY 11973, USA*

† Electronic supplementary information (ESI) available. See DOI: 10.1039/c5cc09434h

Published on 25 February 2016. Downloaded by Iowa State University on 19/09/2016 03:29:56.

The need for this is reinforced by the fact that different results are obtained when nominally identical synthesis methods are used by different groups, owing to the complexity of controlling the $LiNiO_2$ stoichiometry.[16,17]

Herein, we report a comprehensive study on the effect of various solid-state synthesis parameters on the crystal structures, morphologies, and surface characteristics of layered lithium nickel oxides and correlate these characteristics with their electrochemical performance. The best $LiNiO_2$ demonstrated excellent electrochemical performance including high discharge capacity, good rate capability, and capacity retention. This work provides insights into the surface chemistries of $LiNiO_2$ materials and sheds light on the design of Ni-based cathode materials for Li-ion batteries.

$LiNiO_2$ samples were prepared by a solid state method using both commercial and precipitated $Ni(OH)_2$ precursors. The synthesis of $LiNiO_2$ using the precipitated nickel hydroxide precursor followed the protocol originally designed for lithium nickel manganese cobalt oxide.[4,18] For this, 2% and 10% excess LiOH precursors were used; the as-prepared samples are denoted as "solution_2exLi" and "solution_10exLi", respectively. The third sample was simply synthesized following a general solid state reaction protocol by milling Li_2CO_3 and $Ni(OH)_2$ (Sigma Aldrich) precursors with 10% excess Li, henceforth, referred to as "solid_10exLi" (for experimental details, see the ESI†). Fig. 1(a) shows the synchrotron X-ray diffraction (SXRD) patterns of the as-synthesized $LiNiO_2$ powders. The high intensity ratios between (003) and (104) and clear peak splits between (108) and (110) suggest good phase crystallinity and cation ordering,[12] which are further confirmed by the Rietveld refinement results (Table S1, ESI†). Overall, the occupancies of 3a sites by Ni ions are less than 2% for all three samples. Scanning electron microscopy (SEM) images (Fig. 1(b)–(d)) illustrate that the secondary particle size of the as-synthesized powders averages about a few microns, and a relatively uniform particle size distribution was

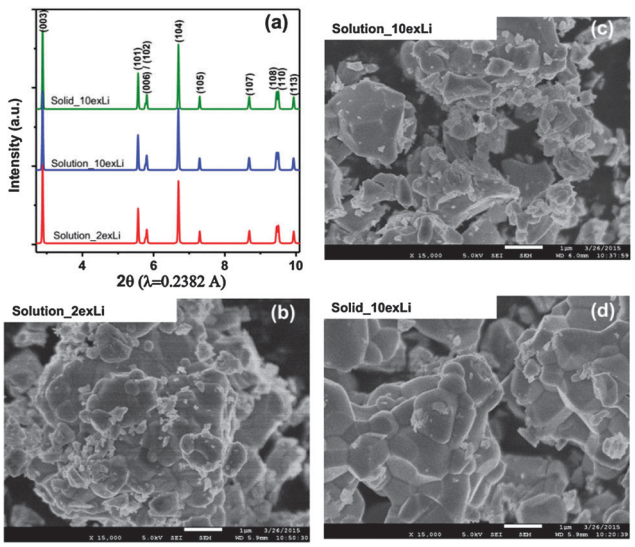

Fig. 1 (a) Synchrotron X-ray diffraction patterns of $LiNiO_2$ prepared from solution_2exLi, solution_10exLi, and solid_10exLi. (b–d) SEM images of the as-prepared powders, respectively.

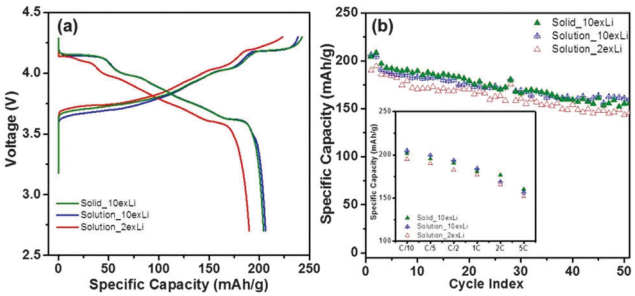

Fig. 2 (a) The 1st cycle voltage profiles, (b) cycling performances, and inset rate capabilities of solution_2exLi, solution_10exLi, and solid_10exLi. Cells were cycled between 4.3 and 2.7 V at C/10, and the capacity at 1C was defined as 180 mA g^{-1}.

observed for the solid_10exLi sample (the histogram is shown in Fig. S1, ESI†).

The materials were cycled between 4.3 and 2.7 V at C/10 for the electrochemical tests. The 1st cycle voltage profiles are shown in Fig. 2(a). Solution_2exLi delivered a capacity of 223 mA h g^{-1} in the first charge, and 190 mA h g^{-1} in the first discharge. The 1st cycle electrochemical behaviors of $LiNiO_2$ prepared with 10% excess Li (solution_10exLi and solid_10exLi) were quite similar, suggesting a negligible effect of the $Ni(OH)_2$ precursor. These two samples delivered a charge capacity of 240 mA h g^{-1} (corresponding to 0.85 Li deintercalation) and a discharge capacity of 206 mA h g^{-1} (corresponding to 0.73 Li re-intercalation). These differences among the samples were repeatable and beyond what would be expected from cell-to-cell variation (<5 mA h g^{-1}) within our experiments, and thus can be considered to result from changing the active material. The higher capacity and lower polarization (as shown in the dq/dV plot in Fig. S2, ESI†) for these two samples compared to those of solution_2exLi indicated that the amount of excess Li in the synthesis had a much larger effect on the electrochemical properties than the source of the Ni precursor. Not only did the larger excess of Li have positive effects on the 1st cycle capacities, but also better rate capability and capacity retention in the subsequent cycles were observed (Fig. 2(b) and inset). After 20 cycles, 88% discharge capacity was maintained, and the retention was still as high as 75% after 50 cycles. Such good performance has rarely been observed for $LiNiO_2$ materials when cycled under similar conditions. In addition, both samples with 10% excess Li exhibited a good rate capability with about 90% capacity retained at 1C. When the current density was further increased, the solid_10exLi sample delivered a slightly higher capacity than solution_10exLi at 2C. This is presumably due to its more uniform particle size distribution as shown by the SEM studies. In contrast, solution_2exLi showed a slightly lower discharge capacity upon cycling and in the rate test as well. Given that SXRD showed similar lattice parameters and cation ordering for these three samples (Table S1, ESI†), such differences observed in the electrochemical performance of the samples synthesized using different amounts of excess Li and different types of $Ni(OH)_2$ precursors must originate from the surface characteristics. To understand these further, surface-sensitive

 This journal is © The Royal Society of Chemistry 2016

Published on 25 February 2016. Downloaded by Iowa State University on 19/09/2016 03:29:56.

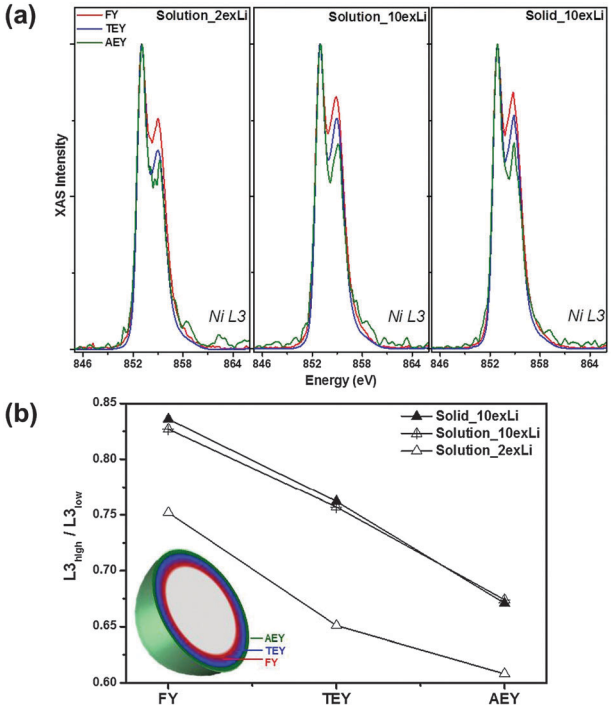

Fig. 3 Soft XAS spectra for three pristine $LiNiO_2$ samples. (a) Ni L3-edge spectra from three detection modes. Note: all the spectra are normalized with respect to the low energy Ni L3-edge. (b) $L3_{high}/L3_{low}$ ratios of all three samples at different modes. The inset illustrates the probing depths for different modes (AEY: 1–2 nm; TEY: 2–5 nm; and FY: ~50 nm).

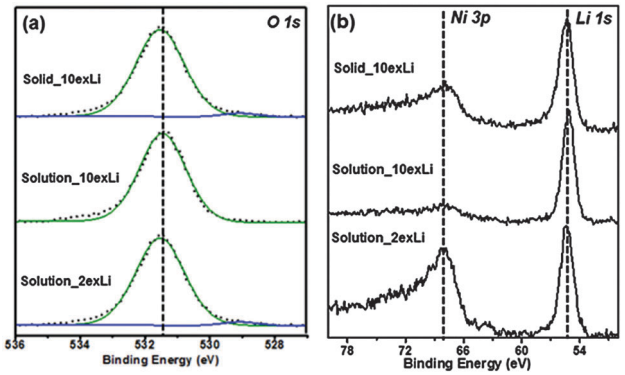

Fig. 4 XPS of (a) O1s regions and (b) Ni3p/Li1s regions for pristine solution_2exLi, solution_10exLi, and solid_10exLi, respectively. Dashed and solid lines in (a) indicate observed and fitted profiles.

soft X-ray absorption spectroscopy (XAS) and X-ray photoelectron spectroscopy (XPS) techniques were employed.

The Ni L3-edge soft XAS spectra of the three pristine powders are shown in Fig. 3. In order to avoid contamination from the adhesive on the carbon tape, all the powders were pressed onto an Au foil for characterization. Three detection modes, Auger electron yield (AEY), total electron yield (TEY), and fluorescence yield (FY), were collected simultaneously. Due to the different mean free paths of electrons and fluorescence in the samples, the AEY, TEY and FY modes typically probe 1–2 nm, 2–5 nm, and ~50 nm from the sample surface towards the bulk, respectively.[4] In other words, information obtained *via* the soft XAS experiment on the as-prepared samples, which have a particle size of about a few microns, concerns both surface (AEY and TEY) and bulk (FY) characteristics of the $LiNiO_2$ materials. For $LiNiO_2$, the most salient electronic structure can be qualitatively obtained through the deconvolution of the Ni L3-edge into high-energy ($L3_{high}$) and low-energy ($L3_{low}$) features. The ratio between $L3_{high}$ and $L3_{low}$ is in a positive relationship with the Ni oxidation state. The three modes (AEY, TEY, and FY) of the Ni L3-edge for each sample shown in Fig. 3(a) are normalized with respect to the $L3_{low}$ feature. It can be clearly seen that the variation in the Ni oxidation state follows a similar trend from the very surface to the sub-surface for all three of the samples. As evidenced by the increased $L3_{high}/L3_{low}$ ratios from the AEY to the FY mode, Ni is more oxidized in the sub-surface region of the $LiNiO_2$ samples compared to their surfaces; in other words, there is an oxidation state gradient. When comparing each mode across the three samples (Fig. 3(b)), it can be seen that solution_2exLi has the lowest Ni oxidation state among all three modes, while the $L3_{high}/L3_{low}$ ratios for the other two samples with 10% excess Li are very close to each other, indicating similar Ni oxidation states and gradients.

In addition to the study on the Ni oxidation state by soft XAS, XPS was also employed to further investigate the surface properties. As can be seen in Fig. 4(a), the main feature of the O1s XPS regions for all three samples is one strong peak at around 531.5 eV, which is associated with Li_2CO_3 on the surfaces.[19,20] The presence of surface Li_2CO_3 is also supported by the following observations: (1) the Li1s peak located at 55.5 eV in Fig. 4(b) and (2) the C1s peak at around 290 eV in the XPS (Fig. S3, ESI†).[19,20] Close examination of the XPS spectra shows the presence of a small peak with very low intensity at 529.5 eV in the solution_2exLi and solid_10exLi samples (Fig. 4(a)), which can be ascribed to the O in the oxide, in this case the lattice of the active material.[19,20] The low intensity of the oxide peak indicates that the reaction layer at the surface is a few nm thick (the O1s XPS was recorded at 670 eV, resulting in a very surface sensitive mean free path of less than 1 nm). The peak is almost invisible in the XPS spectra of the solution_10exLi sample (Fig. 4(a)). In Fig. 4(b), the Li1s and Ni3p XPS region is plotted across the same region for the three samples, and normalized to the Li1s peak intensity. We find a positive correlation between the intensities of O1s peaks corresponding to oxygen in the lattice (529.5 eV) and those due to Ni3p (67.6 eV). The solution_10exLi sample exhibits the lowest intensity Ni3p peak while the O1s in the lattice is almost invisible (Fig. 4(a)). In addition, despite the cross-section difference between Li1s and Ni3p at 670 eV excitation,[21] we would expect to see the typical peak of Li1s at about 53.6 eV associated with the Li in the lattice;[22] however, it is missing in all of the three samples. This directly suggests that the surface Ni atoms exist in a NiO-type phase instead of in layered $LiNiO_2$. In fact, surface NiO-type phase formation in the solution_2exLi sample is correlated with the lower valance state of Ni observed by the soft SXAS experiments because Ni in the NiO phase is

Published on 25 February 2016. Downloaded by Iowa State University on 19/09/2016 03:29:56.

expected to be divalent, whereas it is trivalent in pristine $LiNiO_2$. The combination of XPS and soft XAS results leads to the conclusion that Li_2CO_3 seems to inevitably form on the surface of $LiNiO_2$ even when the amount of excess lithium-containing precursor is small (2%). The lower amount of lithium-excess also results in a stronger tendency to form reduced Ni on particle surfaces, probably in the form of a rock salt phase related to NiO. The main role of a sufficiently large Li-excess during the solid-state synthesis appears to be the suppression of an NiO-type phase formation containing divalent nickel on particle surfaces, which can impede lithium diffusion during cycling, resulting in an inferior electrochemical behavior. The effects of the amount of lithium excess during $LiNiO_2$ synthesis are subtle, affecting primarily the particle surfaces rather than the bulk, which can explain previous results in samples that appear to have similar bulk properties perform differently.

In summary, stoichiometric $LiNiO_2$ with excellent electrochemical performance was synthesized using a solid-state method. The synchrotron XRD results proved that all of the as-prepared $LiNiO_2$ bulk samples were highly crystalline and phase-pure with few defects ($<2\%$ Ni in 3a sites), no matter how much excess lithium was used or what the sources of the $Ni(OH)_2$ starting materials were. However, soft XAS showed that, while Ni tended to be more reduced on the surfaces of all the samples, those samples prepared with a higher amount of excess Li (10%) were less extreme in this regard compared to a sample made with only a 2% excess. This information, in combination with the Li1s, Ni3p, and O1s XPS spectra, can be interpreted to mean that Ni on the surface exists in the form of a NiO-type phase, particularly for the sample made with only a 2% excess of lithium. The XPS O1s and C1s spectra also revealed that Li_2CO_3 preferably formed on the surface of the particles during synthesis even for samples made with a low amount of excess lithium. Both XPS and soft XAS results confirmed the possible formation of a NiO-type phase on the surface, which is inversely correlated to the amount of surface Li_2CO_3 formation. These results indicate that the amount of NiO on the surface can be reduced (although not eliminated entirely) by using a sufficient excess of Li in the synthesis. This study shows a direct correlation between the surface characteristics and superior electrochemical performance, both of which are largely influenced by the amount of excess Li used in the synthesis, and explains why samples with similar bulk properties perform differently. This may also have implications for the syntheses and optimization of other Ni-rich layered oxide cathode materials (*e.g.*, $LiNi_xCo_yAl_{1-x-y}O_2$ and $LiNi_xMn_yCo_{1-x-y}O_2$ $(0 < x, y < 1)$) of interest for battery applications.

This work was supported by the Assistant Secretary for Energy Efficiency and Renewable Energy (EERE), Office of Vehicle Technologies of the U.S. Department of Energy (DOE) under Contract No. DE-AC02-05CH11231. Soft XAS experiments were carried out at the Stanford Synchrotron Radiation Lightsource (SSRL), a Directorate of SLAC National Accelerator Laboratory and an Office of Science User Facility operated for the U.S. DOE Office of Science by Stanford University. The use of the SSRL, SLAC National Accelerator Laboratory, was supported by the U.S. DOE, Office of Science, Office of Basic Energy Sciences under Contract No. DE-AC02-76SF00515. J. Bai and F. Wang thank the support by the U.S. DOE Office of EERE under the Advanced Battery Materials Research program, Contract No. DE-SC0012704. Use of the National Synchrotron Light Source II, Brookhaven National Laboratory, was supported by the U.S. DOE, Office of Science, Office of Basic Energy Sciences, under Contract No. DE-SC0012704. Synchrotron XPS was carried out at beamline 9.3.2 at the Advanced Light Source in Lawrence Berkeley National Laboratory (LBNL), which is supported by the Director, Office of Science, Office of Basic Energy Sciences, of the U.S. DOE under Contract No. DE-AC02-05CH11231. The authors are grateful for the support for Raman characterization from Dr. Robert Kostecki and Dr. Jarry Angelique in LBNL.

References

1 A. Kraytsberg and Y. Ein-Eli, *Adv. Energy Mater.*, 2012, **2**, 922–939.
2 R. V. Chebiam, F. Prado and A. Manthiram, *Chem. Mater.*, 2001, **13**, 2951–2957.
3 F. Lin, D. Nordlund, I. M. Markus, T.-C. Weng, H. L. Xin and M. M. Doeff, *Energy Environ. Sci.*, 2014, **7**, 3077–3085.
4 F. Lin, I. M. Markus, D. Nordlund, T.-C. Weng, M. D. Asta, H. L. Xin and M. M. Doeff, *Nat. Commun.*, 2014, **5**, 3529.
5 H.-J. Noh, S. Youn, C. S. Yoon and Y.-K. Sun, *J. Power Sources*, 2013, **233**, 121–130.
6 Y.-K. Sun, D.-J. Lee, Y. J. Lee, Z. Chen and S.-T. Myung, *ACS Appl. Mater. Interfaces*, 2013, **5**, 11434–11440.
7 J. M. Zheng, W. H. Kan and A. Manthiram, *ACS Appl. Mater. Interfaces*, 2015, **7**, 6926–6934.
8 P. F. Yan, J. M. Zheng, D. P. Lv, Y. Wei, J. X. Zheng, Z. G. Wang, S. Kuppan, J. G. Yu, L. L. Luo, D. Edwards, M. Olszta, K. Amine, J. Liu, J. Xiao, F. Pan, G. Y. Chen, J. G. Zhang and C. M. Wang, *Chem. Mater.*, 2015, **27**, 5393–5401.
9 B. L. Ellis, K. T. Lee and L. F. Nazar, *Chem. Mater.*, 2010, **22**, 691–714.
10 C. Li, H. P. Zhang, L. J. Fu, H. Liu, Y. P. Wu, E. Ram, R. Holze and H. Q. Wu, *Electrochim. Acta*, 2006, **51**, 3872–3883.
11 A. Rougier, P. Gravereau and C. Delmas, *J. Electrochem. Soc.*, 1996, **143**, 1168–1175.
12 T. Ohzuku, A. Ueda and M. Nagayama, *J. Electrochem. Soc.*, 1993, **140**, 1862–1870.
13 C. H. Lu and L. Wei-Cheng, *J. Mater. Chem.*, 2000, **10**, 1403–1407.
14 K. S. Park, S. H. Park, Y. K. Sun, K. S. Nahm, Y. S. Lee and M. Yoshio, *J. Appl. Electrochem.*, 2002, **32**, 1229–1233.
15 H. Arai, S. Okada, H. Ohtsuka, M. Ichimura and J. Yamaki, *Solid State Ionics*, 1995, **80**, 261–269.
16 T. Ohzuku, A. Ueda and M. Nagayama, *J. Electrochem. Soc.*, 1993, **140**, 1862–1870.
17 A. Rougier, P. Gravereau and C. Delmas, *J. Electrochem. Soc.*, 1996, **143**, 1168–1175.
18 F. Lin, D. Nordlund, T. Pan, I. M. Markus, T.-C. Weng, H. L. Xin and M. M. Doeff, *J. Mater. Chem. A*, 2014, **2**, 19833–19840.
19 A. M. Andersson, D. P. Abraham, R. Haasch, S. MacLaren, J. Liu and K. Amine, *J. Electrochem. Soc.*, 2002, **149**, A1358–A1369.
20 N. Yabuuchi, K. Yoshii, S. T. Myung, I. Nakai and S. Komaba, *J. Am. Chem. Soc.*, 2011, **133**, 4404–4419.
21 J. J. Yeh and I. Lindau, *At. Data Nucl. Data Tables*, 1985, **32**, 1–155.
22 M. Oku, H. Tokuda and K. Hirokawa, *J. Electron Spectrosc. Relat. Phenom.*, 1991, **53**, 201–211.

 This journal is © The Royal Society of Chemistry 2016